AIP | Applied Physics Letters

One-dimensional photonic crystal fishbone hybrid nanocavity with nanoposts

Tsan-Wen Lu, Pin-Tso Lin, and Po-Tsung Lee

Citation: Applied Physics Letters **104**, 191107 (2014); doi: 10.1063/1.4876755
View online: http://dx.doi.org/10.1063/1.4876755
View Table of Contents: http://scitation.aip.org/content/aip/journal/apl/104/19?ver=pdfcov
Published by the AIP Publishing

One-dimensional photonic crystal fishbone hybrid nanocavity with nanoposts

Tsan-Wen Lu, Pin-Tso Lin, and Po-Tsung Lee[a)]
Department of Photonics and Institute of Electro-Optical Engineering, National Chiao Tung University, Rm. 413 CPT Building, 1001 Ta-Hsueh Road, Hsinchu 30010, Taiwan

(Received 4 February 2014; accepted 3 May 2014; published online 13 May 2014)

We propose and investigate a one-dimensional photonic crystal (*PhC*) fishbone (*FB*) hybrid nanocavity lying on silver substrate with a horizontal air slot. With very few *PhC* periods, the confined transverse-magnetic, TM_{10} hybrid mode concentrated within the air slot shows high quality factor over effective mode volume ratio larger than $10^5\lambda^{-3}$. Most importantly, this *FB* hybrid nanocavity allows formation of low-index nanoposts within the air slot without significantly affecting the mode properties. These nanoposts guarantee the structural stabilities under different environmental perturbations. Furthermore, capabilities of our proposed design in serving as optical sensors and tweezers for bio-sized nanoparticles are also investigated. © *2014 AIP Publishing LLC*. [http://dx.doi.org/10.1063/1.4876755]

Recently, various one-dimensional (*1D*) photonic crystal (*PhC*) nanocavities on nanobeams[1] (*NBs*) have been proposed and demonstrated for tailoring lightwaves in wavelength scale for different functionalities.[1–5] With high quality factor (Q) and small effective mode volume (V), that is, ultrahigh Q/V, photons can stay in this kind of nanocavities in an enhanced manner for a relatively long time and produce strong light-matter interactions. Owing to small device footprints and high compatibility with waveguides, this kind of nanocavities shows stronger potential in realizing photonic lab-on-chip[6] with higher component density than two-dimensional (*2D*) *PhC* nanocavities. In addition to transverse-electric (*TE*) polarized modes, transverse-magnetic (*TM*) modes are also supported by *1D PhC NB* nanocavities.[7] Unlike the low Q *TM* modes in discontinuous *2D* nanorod nanocavities, the *TM* modes in *1D PhC NB* nanocavities have relatively high Q ($>10^6$). Very recently, a different *1D PhC* fishbone (*FB*) nanocavity[8] design utilizing high-order TM_{10} mode has also been proposed. It shows higher Q ($>10^7$), smaller V, further minimized device volume and footprint than those of reported *PhC NB* nanocavities. Moreover, its significantly reduced etched surface area is very beneficial for reducing non-radiative recombination in active photonic devices.

However, degraded Q/V is inevitable when we further minimize the device footprints of *1D PhC NB* and *FB* nanocavities via reducing *PhC* periods. This is caused by the nature of Q dependence on *PhC* periods. Fortunately, V is almost independent of *PhC* periods. Therefore, reducing V is feasible to maintain sufficiently high Q/V in a *1D PhC* nanocavity with very few *PhC* periods. Generally, there are two approaches to efficiently reduce V in a *TM* polarized *PhC NB* nanocavity. The first one is embedding a horizontal low-index slot[9,10] in *PhC NB*, named slotted nanocavity, as shown in Fig. 1(a). Because the electric displacement has to be continuous when crossing the index discontinuity caused by the slot, E_z field will be significantly enhanced within the slot, which results in a greatly reduced V. However, this approach leads to significantly degraded Q when the slot becomes thick. But thick slot is favorable for optical sensors and tweezers. The second approach is directly putting *PhC NB* nanocavity on a metal substrate,[11] named plasmonic nanocavity, as shown in Fig. 1(b). This structure confines the surface plasmon polariton (*SPP*) wave with sub-wavelength field concentration originated from free electron oscillation at the dielectric/metal interface.[12] However, Q of this kind of plasmonic mode is quite low, limited to the loss from metal.

In this report, via finite-element method[13] (*FEM*), we propose and investigate a *TM* polarized *1D PhC FB* hybrid nanocavity lying on silver substrate with a horizontal air slot. This plasmonic-photonic hybrid structure[14,15] confines a hybrid mode coupling between *SPP* wave and photonic mode within the air slot. With very few *PhC* periods, high Q/V is obtained. In addition, without significantly affecting the mode properties, low-index nanoposts can be formed within the air slot to provide structural stability for the nanocavity under different environmental perturbations. Moreover, capabilities of this hybrid nanocavity in serving as optical bulk index sensors and optical tweezers for bio-sized nanoparticles are also investigated.

1D PhC FB is formed via periodic half air holes on both sides of a ridge waveguide suspending in the air. Its lattice parameters are defined in Fig. 1(c), including air-hole radius r, lattice constant a, *FB* width w, and *FB* thickness t. In this *PhC FB*, we are interested in its high-order TM_{10} mode with high dielectric confinement factor and significant slow light effect at the photonic band edge.[8] Theoretic TM_{10} mode in $|E_z|^2$ at xy- and yz-planes is shown in Fig. 1(c).

A schematic of our proposed *PhC* plasmonic-photonic hybrid *FB* on silver substrate with a horizontal air slot (with thickness g) is shown in Fig. 2(a). In this *PhC* hybrid *FB*, we design a nanocavity according to the principle of Bloch mode index matching,[1] as illustrated in Fig. 2(b). Under fixed half air-hole radius (r_n) over a_n (r_n/a_n) ratio of 0.32, the lattices are arranged to have a 3-period *PhC* outer mirror with fixed a and a 6-period gradually varied *PhC* tapered mirror with lattice constant $a_n = (1 - 0.02n)a$ ($n = 1$ to 6) on each side of *PhC FB* nanocavity. This nanocavity design

a)Electronic mail: potsung@mail.nctu.edu.tw

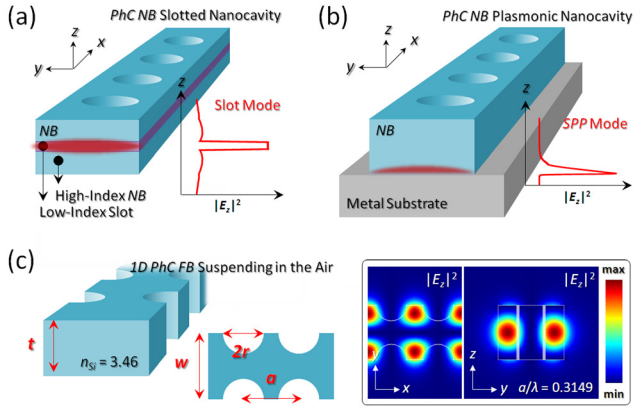

FIG. 1. Schematic illustrations of two approaches to reduce V in TM polarized PhC NB nanocavities, (a) nanocavity with embedded horizontal low-index slot and (b) plasmonic nanocavity directly on a metal substrate. (c) Schematic and parameters of $1D$ PhC FB suspending in the air and its theoretic TM_{10} mode in $|E_z|^2$ at xy- and yz-planes.

strongly confines the TM_{10} hybrid mode originating from the coupling between SPP wave and TM_{10} mode at the photonic band edge (where $k_x = 0.5(2\pi/a)$). The dielectric function of silver substrate in this hybrid nanocavity is described by $Drude$ model[16] in three-dimensional ($3D$) FEM. The background dielectric constant ε_∞, plasma frequency ω_p, and collision frequency γ are set as 5, 1.38×10^{16} rad/s, and 5×10^{13} rad/s for optical communication wavelength. For PhC FB hybrid nanocavity with t, w, and g of $0.84a$, a, and $0.05a$, the TM_{10} hybrid mode in $|E_z|^2$ at yz- and xy-planes is shown in Fig. 2(c), with strong field concentration within the air slot. High Q of 2500 and extremely small V of $0.016\lambda^3$ lead to a very high Q/V of $1.56 \times 10^5 \lambda^{-3}$, where $\lambda = \lambda_0/n_{max}$ and n_{max} is the index of the region with maximum field.

First, we investigate the dependences of Q and V on air slot thickness g, as shown in Figs. 2(d) and 2(e). Two mechanisms are responsible for the loss (Q^{-1}) of TM_{10} hybrid mode, namely, radiation loss (Q_r^{-1}) from PhC FB hybrid nanocavity and metal absorption loss (Q_a^{-1}) from the silver substrate, that is, $Q^{-1} = Q_r^{-1} + Q_a^{-1}$. In Fig. 2(d), under different g, Q_a is always much lower than Q_r and dominates Q. Increased g leads to reduced scattering losses caused by the substrate, which results in increased Q_r. In addition, when g increases, loss from the metal absorption decreases because of the weakened coupling strength between SPP wave and photonic mode, which leads to significantly increased Q_a. When g is much larger than the coupling length (equivalent to a PhC FB nanocavity suspending in the air), the TM_{10} hybrid mode shows $Q_a \sim \infty$ and $Q \sim Q_r = 8.5 \times 10^4$. However, weakened coupling strength caused by increased g also means that the mode energy will be pulled from the air slot back into PhC FB. This mode energy pulling-back leads to enlarged V and smoothly decreased Q/V, as shown in Fig. 2(e). When $g = 0.025a$ (for $a = 400$ nm, $g = 10$ nm), V is as small as $0.007\lambda^3$ and Q is 1400, which results in a very high Q/V of $2 \times 10^5 \lambda^{-3}$.

We then investigate Q and V variations when the device size is further minimized via reducing the number of PhC periods P from 11 to 4. Here, $P = 11$ means the nanocavity has 6-period tapered and 5-period outer mirrors on each side, and $P = 4$ means only 4-period tapered mirror with lattices from a_6 to a_3. With t, w, and g of $0.84a$, a, and $0.05a$, respectively, Q, Q_r, and Q_a of the TM_{10} hybrid modes in PhC FB hybrid nanocavities with different P are shown in Fig. 3(a). Because g is fixed, constant metal loss leads to invariant Q_a (~2600). However, Q_r monotonically decreases with reducing P because of weakened photonic band gap confinement.

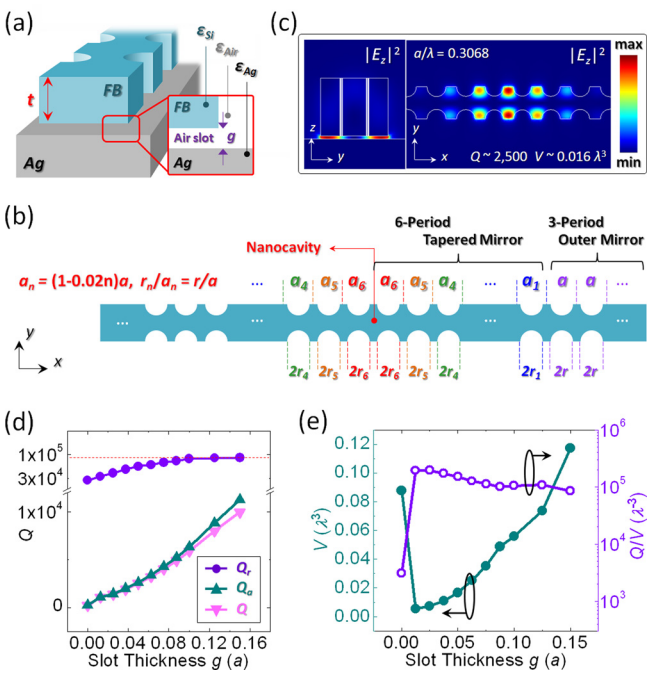

FIG. 2. (a) Schematic and parameters of PhC hybrid FB on silver substrate with a horizontal air slot. (b) Design of PhC FB hybrid nanocavity with the tapered and outer mirrors. (c) $|E_z|^2$ of the TM_{10} hybrid mode at yz- and xy-planes shows strong field concentration within the air slot of PhC FB hybrid nanocavity. Theoretic (d) Q, Q_r, Q_a, (e) V, and Q/V of the TM_{10} hybrid modes in PhC FB hybrid nanocavities with different air slot thicknesses g.

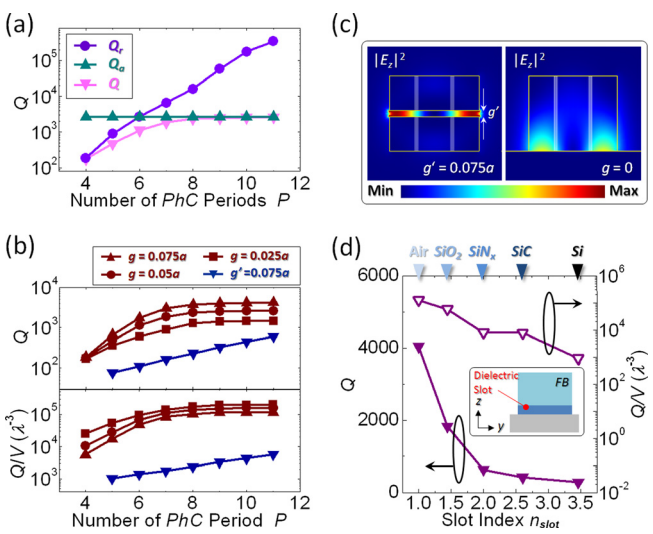

FIG. 3. (a) Theoretic Q, Q_r, and Q_a of the TM_{10} hybrid modes in PhC FB hybrid nanocavities with different P. (b) Theoretic Q and Q/V of the TM_{10} hybrid modes in PhC FB hybrid nanocavities with different g and P. The solid lines with inverse triangles denote Q and Q/V of the TM_{10} modes in PhC FB slotted nanocavities with $g' = 0.075a$. (c) TM_{10} mode profiles in $|E_z|^2$ at yz-plane confined in PhC FB slotted and plasmonic nanocavities. (d) Theoretic Q and Q/V of the TM_{10} hybrid modes in PhC FB hybrid nanocavities with different n_{slot}.

Therefore, Q is dominated by Q_r when $P<6$ but dominated by Q_a when $P>6$. When $P>7$, Q becomes saturated and is almost equal to Q_a. Fig. 3(b) shows Q and Q/V of the TM_{10} hybrid modes in *PhC FB* hybrid nanocavities with different P when g are $0.025a$, $0.05a$, and $0.075a$. Since V is almost invariant under different P, the variation of Q/V follows that of Q, that is, Q/V decreases with reducing P. With $P=4$ and $g=0.025a$, high $Q/V\sim2.5\times10^4\lambda^{-3}$ of the TM_{10} hybrid mode is still obtained.

For comparison, we apply the two approaches shown in Figs. 1(a) and 1(b) separately to the *PhC FB* nanocavity to reduce V. For *PhC FB* slotted nanocavity with embedded air slot (with thickness g'), both Q and V significantly degrade when g' increases, which leads to a fast decrease in Q/V. As shown in Fig. 3(b), with $g'=0.075a$ and optimized lattice parameters, *PhC FB* slotted nanocavities show more than one order lower Q/V than *PhC FB* hybrid nanocavities with the same P. In addition, for *PhC FB* plasmonic nanocavity directly on silver substrate ($g=0$), Q is dominated by the metal loss from silver. This domination leads to a limited $Q\sim Q_a\sim270$ and results in a relatively low Q/V of 3000 while V is $0.09\lambda^3$, as shown in Figs. 2(d) and 2(e). Theoretic TM_{10} modes in $|E_z|^2$ at yz-plane in *PhC FB* slotted and plasmonic nanocavities are shown in Fig. 3(c).

In fabrication, the air slot of *PhC FB* hybrid nanocavity can be realized via selectively wet etching a pre-deposited dielectric slot between *PhC FB* and metal substrate, shown as the inset in Fig. 3(d). This dielectric slot can be made via sputtering, chemical vapor deposition, or atom layer deposition with nano- or sub-nanometer precision in thickness. Therefore, dielectric slot with $g<10$ nm can be easily and precisely achieved. This is very different from the vertical slot width in *TE* polarized *PhC* nanocavities[17] limited by electron beam lithography and dry etching processes. Furthermore, for light emitting applications, various optical gain mediums (for example, earth-rare dopant and germanium) can be embedded in the dielectric slot during deposition process.[18,19] For *PhC FB* hybrid nanocavities with fixed $g=0.075a$ and different dielectric slots with indices n_{slot} ranged from 1.0 to 3.46 (for example, air, SiO_2, SiN_x, SiC, and Si), Q and Q/V of the TM_{10} hybrid modes both decrease when n_{slot} increases, as shown in Fig. 3(d). Increased n_{slot} leads to increased index of the *SPP* mode at the slot-sliver interface (n_{SPP}, defined as $(\varepsilon_m\varepsilon_{slot}/(\varepsilon_m+\varepsilon_{slot}))^{1/2}$, where ε_m and ε_{slot} are the permittivities of silver substrate and slot). The increased n_{SPP} results in a reduced difference between n_{SPP} and the effective index of *NFB* cavity mode. This enhances hybrid mode coupling between the *NFB* cavity mode and *SPP* mode.[14] And the enhanced hybrid mode coupling means increased metal loss from the *SPP* mode, which leads to decreased Q. However, for *PhC FB* hybrid nanocavity with SiO_2 ($n_{slot}=1.44$) slot, Q/V of the TM_{10} hybrid mode is still as high as $10^5\lambda^{-3}$. This high Q/V provides strong light-matter interactions when embedding gain medium in SiO_2 slot for active light emitters.

Although thin air slot can compress mode energy inside, it also makes the *PhC FB* hybrid nanocavity structurally unstable because of the perturbations from optical force interacting with the substrate[20] or environmental fluids (capillary force) in bio-sensing and trapping applications. To prevent *PhC FB* from sticking on silver substrate, forming dielectric nanoposts (for example, SiO_2 with low index) within the air slot as shown in Figs. 4(a) and 4(b) is proposed. Owing to central zero-field distribution of the TM_{10} hybrid mode shown in Fig. 2(c), these nanoposts will not significantly affect the TM_{10} hybrid mode properties. In fabrication, via carefully controlling wet etching time[21] or wet etching rate[22] via diluted hydrofluoric acid solutions, we can obtain SiO_2 nanoposts with different diameters within the air slot. Topology of the SiO_2 nanoposts with diameter D after lateral wet etching is illustrated in Fig. 4(b). With different D, Q of the TM_{10} hybrid modes is almost invariant when $D\leq0.4a$ and decreases when $D>0.4a$, as shown in Fig. 4(c). When $D>0.4a$, the mode overlapping with the SiO_2 nanoposts (γ_{post}, defined as the ratio of energy concentrated in SiO_2 nanoposts) increases, as shown in Fig. 4(c). This means equivalently increased n_{slot} and leads to increased metal loss as we discussed in Fig. 3(d). Theoretic TM_{10} hybrid modes in $|E_z|^2$ at yz-plane in *PhC FB* hybrid nanocavities with $D=0.4a$ and $0.8a$ are shown in Fig. 4(d). Therefore, we can conclude that the SiO_2 nanoposts with $D\leq0.4a$ can provide structural stabilities for the *PhC FB* hybrid nanocavity without significantly affecting the TM_{10} hybrid mode properties.

We then investigate the capabilities of TM_{10} hybrid mode in *PhC FB* hybrid nanocavity for optical bulk index sensing. D and P of the nanocavity are set as $0.4a$ and 6 for mechanical support and compact device size. Via changing the environmental refractive index (including the slot region), theoretic index sensitivity R_n (wavelength shift per refractive index unit (*RIU*) change, nm/*RIU*) and corresponding figure of merit (*FOM*, defined as ratio of R_n to width of resonance peak) are shown in Fig. 5(a). Introducing air slot brings more mode energy distribution in the air. Therefore, a dramatic increase in R_n is observed in Fig. 5(a) when g becomes larger than zero. And R_n starts to slowly decrease when $g>0.075a$ because the mode energy is pulled from the air back to *PhC FB*. Furthermore, because Q increases with g and becomes saturated ($\sim$1900) when $g>0.075a$, we can

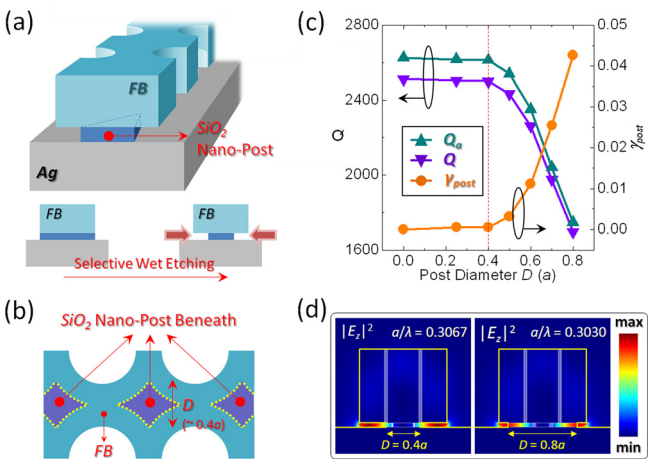

FIG. 4. (a) Schematic of SiO_2 nanoposts formed within the air slot of *PhC FB* hybrid nanocavity. (b) Topology of the nanoposts with diameter D within the air slot. (c) Theoretic Q, Q_a, and γ_{post} of the TM_{10} hybrid modes in *PhC FB* hybrid nanocavities with different D. (d) TM_{10} hybrid modes in $|E_z|^2$ at yz-plane in *PhC FB* hybrid nanocavities with $D=0.4a$ and $0.8a$.

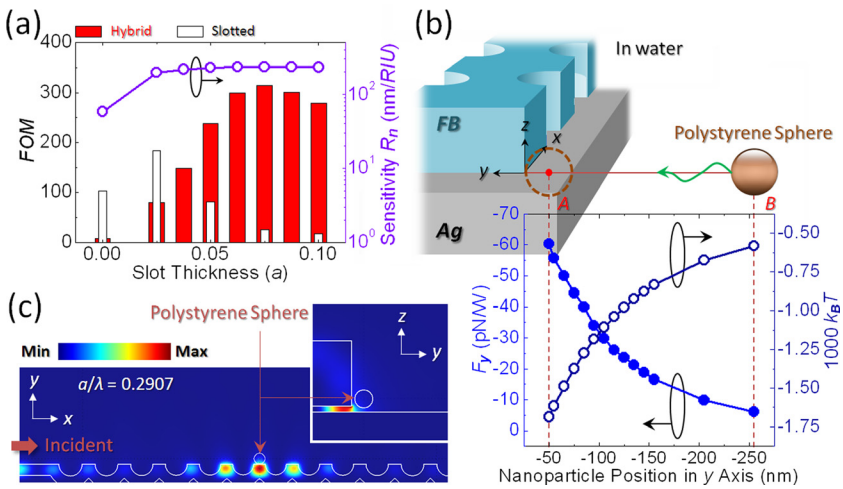

FIG. 5. (a) Theoretic R_n and *FOM* of *PhC FB* hybrid nanocavities with fixed $P=6$ and different g. (b) Schematic, trapping force, and optical potential of TM_{10} hybrid mode in *PhC FB* hybrid nanocavity with $g=0.075a$ for a *PS* with radius of 50 nm. (c) Theoretic TM_{10} hybrid mode in $|E_z|^2$ at *xy*- and *yz*-planes when the *PS* is trapped at position *A*.

obtain a maximum *FOM* of 315 when $g=0.075a$. For comparison, with the same parameters, *PhC FB* plasmonic nanocavity ($g=0$) shows very low *FOM* of 8. Although high *FOM* of 180 is obtained from *PhC FB* slotted nanocavity with $g'=0.025a$, it rapidly decreases when g' increases because of fast degraded Q, as denoted via the white columns in Fig. 5(a).

In addition to index sensing, we also show the capabilities of *PhC FB* hybrid nanocavity in optically trapping bio-sized nanoparticle in fluidics.[3,23,24] In *3D FEM* simulations, the hybrid nanocavity is assumed to be immersed in water with index of 1.33. And the target polystyrene sphere (*PS*) with index of 1.59 and size of 50 nm in radius mimics the viruses for diseases of the respiratory system, for example, Influenza *A* (*H1N1*) virus, corona virus for severe acute respiratory syndrome (*SARS*), and so on. The trapping force given by the TM_{10} hybrid mode on the *PS* is calculated via *Maxwell* stress tensor.[23] As illustrated in Fig. 5(b), the trapping force along *y*-axis (F_y) becomes stronger when the *PS* gets closer to the slot ($g=0.075a=30$ nm for $a=400$ nm) within which the TM_{10} hybrid mode concentrates. Via in-plane light incident power of 1 *W*, Fig. 5(c) shows TM_{10} hybrid mode in $|E_z|^2$ at *xy*- and *yz*-planes when the *PS* is stably trapped at position *A* (as denoted in Fig. 5(b)), where F_y is as strong as 60 *pN/W*. We further integrate the attractive force along the path from *B* to *A* to obtain the corresponding optical potential energy *U* experienced by the *PS*, as shown in Fig. 5(b). It shows a potential well $\Delta U > 1100 k_BT$ along the path, where k_B and *T* are *Boltzmann* constant and temperature (set as 300 *K*). This ΔU is much larger than $10k_BT$, which can overcome *Brownian* motion and guarantee stable trapping.[24]

In summary, we propose and investigate a *1D PhC FB* hybrid nanocavity lying on silver substrate with a horizontal air slot. With very few *PhC* periods, the confined TM_{10} hybrid mode shows high Q/V over $10^5\lambda^{-3}$. Most importantly, this *PhC FB* hybrid nanocavity allows the formation of low-index (SiO_2) nanoposts with $D \leq 0.4a$ within the air slot without significantly affecting TM_{10} hybrid mode properties. These nanoposts also guarantee structural stabilities for the nanocavity under different environmental perturbations. Moreover, our presented design shows high *FOM* of 315 in optical bulk index sensing and strong optical trapping force of 60 *pN/W* for bio-sized nanoparticle (50 nm in radius) in fluidics. We believe this kind of *PhC FB* hybrid nanocavity with compact device size and strong light-matter interaction can be used to develop efficient nanolasers, optical sensors, and biologic manipulators.

This work was supported by Taiwan's National Science Council (NSC) under Contract Nos. NSC-100-2221-E-009-109-MY3 and NSC-101-2221-E-009-054-MY2.

[1]Y. Zhang, M. Khan, Y. Huang, J. H. Ryou, P. B. Deotare, R. Dupuis, and M. Lončar, Appl. Phys. Lett. **97**, 051104 (2010).
[2]B. Wang, M. A. Dündar, R. Nötzel, F. Karouta, S. He, and R. W. van der Heijden, Appl. Phys. Lett. **97**, 151105 (2010).
[3]Y. F. Chen, X. Serey, R. Sarkar, P. Chen, and D. Erickson, Nano Lett. **12**, 1633 (2012).
[4]P. B. Deotare, L. C. Kogos, I. Bulu, and M. Lončar, IEEE J. Sel. Top. Quantum Electron. **19**, 3600210 (2013).
[5]X. Chew, G. Zhou, F. S. Chau, J. Deng, X. Tang, and Y. C. Loke, Opt. Lett. **35**, 2517 (2010).
[6]C. Monat, P. Domachuk, and B. J. Eggleton, Nat. Photonics **1**, 106 (2007).
[7]M. W. McCutcheon, P. B. Deotare, Y. Zhang, and M. Lončar, Appl. Phys. Lett. **98**, 111117 (2011).
[8]T. W. Lu and P. T. Lee, Opt. Lett. **38**, 3129 (2013).
[9]J. T. Robinson, K. Preston, O. Painter, and M. Lipson, Opt. Express **16**, 16659 (2008).
[10]T. W. Lu, P. T. Lin, and P. T. Lee, Opt. Lett. **37**, 569 (2012).
[11]M. K. Kim, S. H. Lee, M. Choi, B. H. Ahn, N. Park, Y. H. Lee, and B. Min, Opt. Express **18**, 11089 (2010).
[12]J. A. Schuller, E. S. Barnard, W. Cai, Y. C. Jun, J. S. White, and M. L. Brongersma, Nature Mater. **9**, 193 (2010).
[13]COMSOL Multiphysics software package.
[14]R. F. Oulton, V. Sorger, D. A. Denov, D. F. P. Pile, and X. Chang, Nat. Photonics **2**, 496 (2008).
[15]D. Dai and S. He, Opt. Express **17**, 16646 (2009).
[16]P. B. Johnson and R. W. Christy, Phys. Rev. B **6**, 4370 (1972).
[17]M. G. Scullion, T. F. Krauss, and A. Di Falco, Sensors **13**, 3675 (2013).
[18]C. Creatore, L. C. Andreani, M. Miritello, R. Lo Savio, and F. Priolo, Appl. Phys. Lett. **94**, 103112 (2009).
[19]J. M. Ramírez, F. F. Lupi, Y. Berenćen, A. Anopchenko, J. P. Colonna, O. Jambois, J. M. Fedeli, L. Pavesi, N. Prtljaga, P. Rivallin, A. Tengattini, D. Navarro-Urrios, and B. Garrido, Nanotechnology **24**, 115202 (2013).
[20]J. Ma and M. L. Povinelli, Appl. Phys. Lett. **97**, 151102 (2010).
[21]W. D. Ho, T. W. Lu, Y. H. Hsiao, and P. T. Lee, J. Lightwave Technol. **27**, 5302 (2009).
[22]M. K. Seo, K. Y. Jeong, J. K. Yang, Y. H. Lee, H. G. Park, and S. B. Kim, Appl. Phys. Lett. **90**, 171122 (2007).
[23]A. H. J. Yang and D. Erickson, Nanotechnology **19**, 045704 (2008).
[24]S. Lin, J. Hu, L. Kimerling, and K. Crozier, Opt. Lett. **34**, 3451 (2009).